PHOTONICS Research

Ultra-high-Q resonances in terahertz all-silicon metasurfaces based on bound states in the continuum

Pengfei Wang, Fengyan He, Jianjun Liu, Fangzhou Shu, Bin Fang, Tingting Lang, Xufeng Jing, and Zhi Hong*

Centre for THz Research, China Jiliang University, Hangzhou 310018, China
**Corresponding author: hongzhi@cjlu.edu.cn*

Received 15 July 2022; revised 10 October 2022; accepted 12 October 2022; posted 14 October 2022 (Doc. ID 470657); published 22 November 2022

High-Q metasurfaces have important applications in high-sensitivity sensing, low-threshold lasers, and nonlinear optics due to the strong local electromagnetic field enhancements. Although ultra-high-Q resonances of bound states in the continuum (BIC) metasurfaces have been rapidly developed in the optical regime, it is still a challenging task in the terahertz band for long years because of absorption loss of dielectric materials, design, and fabrication of nanostructures, and the need for high-signal-to-noise ratio and high-resolution spectral measurements. Here, a polarization-insensitive quasi-BIC resonance with a high-Q factor of 1049 in a terahertz all-silicon metasurface is experimentally achieved, exceeding the current highest record by 3 times of magnitude. And by using this ultra-high-Q metasurface, a terahertz intensity modulation with very low optical pump power is demonstrated. The proposed all-silicon metasurface can pave the way for the research and development of high-Q terahertz metasurfaces.

https://doi.org/10.1364/PRJ.470657

1. INTRODUCTION

Bound states in the continuum (BICs) are bound states that lie inside the continuum. Under such states the energy can be perfectly confined within the system and without any radiation. Therefore, a BIC can be considered as a resonance with zero linewidth or an infinite Q factor [1,2]. In theory, BICs are dark modes with infinite radiative lifetime, which are "invisible" for far-field measurement, but they can be observed at near-field experiments [3]. However, due to the finite size of structures, material absorption, and other external perturbations, BICs tend to collapse to a Fano resonance with a limited radiative Q factor; such resonances are known as quasi-BICs [4–6]. There are two main types of BICs in metamaterials: symmetry protected BIC [1] and Friedrich–Wintgen (F–W) BIC [7]. The coupling coefficient could vanish due to the symmetry reason when the spatial symmetry of the mode is incompatible with the symmetry of the outgoing radiating waves. This kind of BIC is called symmetry protected BIC. The ideal symmetry protected BIC can be transformed into quasi-BIC by constructing a radiation channel through oblique incidence or breaking the structural symmetry [8–11], while the F–W BIC is generated by the destructive interference of the two eigenmodes, which requires precise adjustment of parameters of the structure. If the structural parameters deviate from the ideal BIC point, it becomes a quasi-BIC with a finite Q value [12–18]. In addition, BICs can be found and originated from guided mode resonances (GMRs) or surface lattice resonance in dimer or multimer configurations [19–22]. They become GMRs or bright modes (electric and magnetic dipole modes) with a finite Q factor when the lattice symmetry is broken by changing the position or size of its building blocks. A BIC provides a new way for the realization of high-Q metasurfaces and has been applied in high-sensitivity sensing [23–26], low-threshold micro-nano lasers [27,28], and nonlinear harmonic generations [29,30].

In metasurfaces, high-Q Fano resonance was mainly obtained by breaking the symmetry of the structure [31–34], and its Q value was determined by the asymmetry parameter of the structure. Theoretically, the smaller the asymmetry degree, the higher Q value of the metasurface. Hence, metasurfaces with arbitrary high Q value can be easily designed. However, it is very difficult to be achieved in experiments. So far, the reported highest Q value in the terahertz (THz) band is 227 [32], and 1011 in the optical regime [35–37]. In addition, high-Q resonances can also be achieved by exploiting surface lattice resonances in the symmetrical plasmonic metasurface, and a Q value of 2340 was obtained experimentally at the optical wavelengths [38–40]. Recent research on BICs has greatly

promoted the development of high-Q dielectric metasurface with both symmetric and asymmetric structures, especially at optical frequencies [12,41–44]. For example, in a silicon cubic metasurface supporting symmetry protected BIC, a Q value of a quasi-BIC obtained reached up to 18,511 [43], and meanwhile, optical second and third nonlinear harmonics were observed simultaneously. However, it remains challenging for long years to achieve high-Q resonances in terahertz metasurfaces because of the absorption loss of dielectric materials, the design and fabrication of nanostructures, and high-signal-to-noise ratio high-resolution spectral measurements. To date, the highest Q value reported experimentally is only 250 in a silicon BIC terahertz metasurface [14].

In this work, we investigate and experimentally demonstrate an ultra-high-Q quasi-BIC resonance in an all-silicon metasurface with perforated air hole tetramers. The metasurface supports two BICs originated from GMRs in a frequency range of 0.4–0.9 THz, which collapses into two quasi-BIC Fano resonances with finite Q values through changing the radius of air holes in diagonal configuration. Thanks to the designed metasurface with strong coupling of the unit cells and without substrate avoiding material absorption loss, we successfully achieved a polarization-insensitive quasi-BIC with a record Q factor as high as 1049 in experiments. Further, we demonstrate a terahertz intensity modulation with very low optical pump power by exploring photon-induced carrier absorption of semiconductors. The perforated air-hole all-silicon terahertz metasurfaces have been rarely reported experimentally [45,46]. The work in this paper could pave the way not only for the research and application of high-Q terahertz metasurfaces, but also for other functional devices [47,48].

2. STRUCTURE DESIGN AND SIMULATION RESULTS

An all-dielectric metasurface we designed consists of perforated air-hole tetramers arrays in a high-resistance silicon wafer shown in Fig. 1. The all-silicon metasurface without substrate is compatible with the CMOS technique and ease of fabrication; meanwhile, its Q factor can be improved by avoiding the material absorption loss of the substrate.

In Fig. 1, the radii of the air holes at the two diagonals are represented by r_1 and r_2, respectively, and the thickness of the silicon wafer is 150 μm. The periods of the unit cell in the x and y directions are $\Lambda_x = \Lambda_y = \Lambda = 300$ μm, and the distance between the centers of the two circles along the x and y directions is fixed at $\Lambda/2 = 150$ μm. Numerical simulations were carried out using the finite element method (COMSOL Multiphysics software), in which periodic boundary conditions are employed in the x and y directions, a perfectly matched layer is employed in the z direction, and the dielectric constant of silicon is set to be 11.67.

First, at fixed $r_2 = 55$ μm, the transmission spectra of metasurfaces with different r_1 were calculated and shown in Fig. 2(a). There are three strong Fano resonances in the range of 0.4–0.9 THz, marked as f_1, f_2, and f_3, respectively. The resonance frequencies and Q factors of f_1 and f_2 are shown in Figs. 2(b) and 2(c), and Q values are extracted from transmissions by Fano fitting as [49,50]

$$T(\omega) = T_0 + A_0 \frac{[q + 2(\omega - \omega_0)/\gamma]^2}{1 + [2(\omega - \omega_0)/\gamma]^2}, \tag{1}$$

where q is the Fano fitting parameter that determines the asymmetry of the resonance curve, ω_0 and γ represent the resonance peak angular frequency and the resonance linewidth, respectively, T_0 is the transmittance baseline shift, and A_0 is the coupling coefficient, therefore, $Q = \omega_0/\gamma$.

As r_1 increases from 25 to 75 μm, the three resonances have obvious blueshifts, due to the decrease of the effective refractive index of the metasurface. In particular, for a symmetric metasurface when $r_1 = r_2 = 55$ μm, both resonances f_1 and f_2 located at ~0.577 THz and 0.739 THz, respectively, disappear, i.e., the Q factor is infinite. Moreover, on both sides of $r_1 = 55$ μm, when r_1 is away from 55 μm, the Q factors of f_1 and f_2 decrease dramatically, showing typical BIC characteristics. While the resonance f_3 is very different from f_1 and f_2, its Q factor decreases rapidly as r_1 increases from 25 to 75 μm and is finite when $r_1 = 55$ μm. In addition, when r_1 is in the range of 25–40 μm, the Q value of f_1 is much larger than that of f_2; while in the range of 60–75 μm, the Q value of f_1 is just slightly higher than that of f_2. Moreover, the transmittances of the two quasi-BIC resonances are polarization-insensitive according to the geometrical symmetry of the structure.

To interpret the physical origin of the three resonances, the related intrinsic band structures of the TE and TM modes from the metasurfaces at lattice constants of 300 μm and 150 μm were investigated by COMSOL Multiphysics.

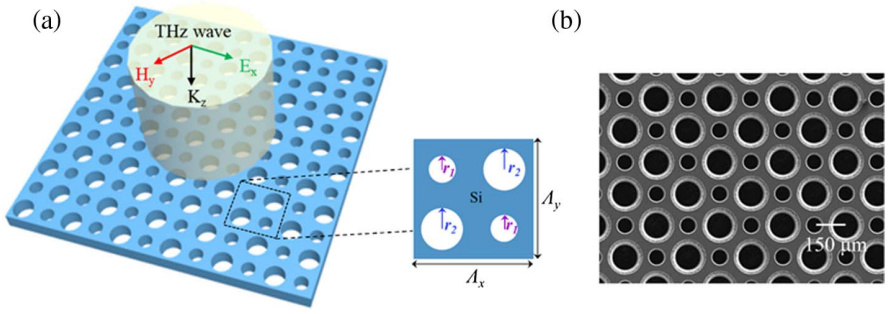

Fig. 1. (a) Schematic diagram of a high-Q all-silicon terahertz metasurface consisting of periodic air-porous tetramers. The periods of the unit cell are $\Lambda_x = \Lambda_y = \Lambda = 300$ μm, and the thickness of the metasurface is 150 μm. (b) SEM picture of one fabricated metasurface when $r_1 = 35$ μm, $r_2 = 55$ μm.

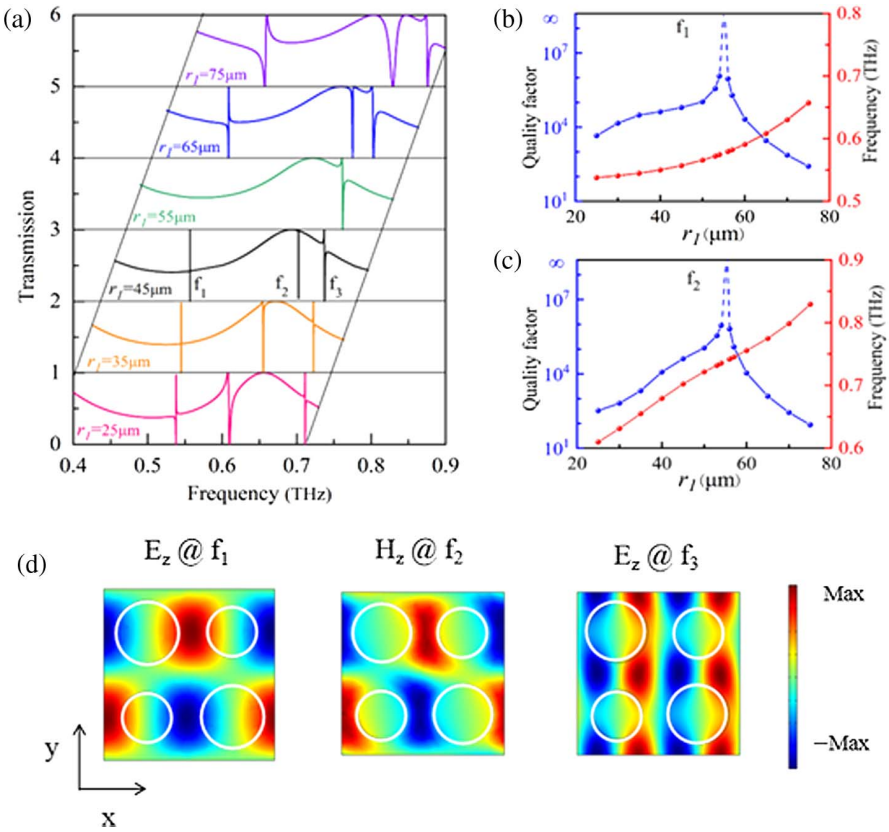

Fig. 2. (a) Calculated transmissions of metasurfaces with different r_1 when $r_2 = 55$ μm, where three Fano resonances are marked as f_1, f_2, and f_3. (b), (c) Resonance frequencies and Q factors of f_1, f_2 with respect to r_1. (d) Electric field (E_z) or magnetic field (H_z) of resonance f_1, f_2, and f_3, when $r_1 = 45$ μm.

Here, $r_1 = r_2 = 55$ μm; thus, the metasurface with a lattice constant of 300 μm degenerates to a metasurface with a lattice constant of 150 μm. As we can see from the TE modes in Fig. 3(a), the band structure of the 300 μm-period unit cell (blue line) is folded from that of the 150 μm-period unit cell (red line). Meanwhile, bound states in the discrete region of the 150 μm-period unit cell would be folded inside the light cone, which results in bound states in the continuum [20–22]. From the enlarged view of our considered modes, there are two eigenmodes TE 1 and TE 2 (related to f_2), both with infinite Q factors at Γ point and off Γ point (not shown in the figure), which does not exist at the lattice constant of 150 μm. Considering their magnetic field distributions at Γ point in Fig. 3(c), it can be inferred that the two TE modes are BICs originated from GMRs induced by (1, 1) Rayleigh diffraction from a two-dimensional (2D) metagrating at a 300 μm lattice constant, and propagating along 45° and −45° to the x axis [20,51,52]. And resonance f_2 is the result of the co-excitation of these two GMRs.

Similar to the above two TE modes, two TM modes (related to f_1), TM 1 and TM 2, both with infinite Q factor at Γ point and off Γ point, only exist in the metasurface at the lattice constant of 300 μm [shown in Fig. 3(b)]; they are two BICs originated from GMRs propagating along 45° and −45° to the x axis, as shown in Fig. 3(c). In addition, TM 3 and TM 4 are two GMRs induced by (1, 1) Rayleigh diffraction from a 2D metagrating at 300 μm lattice constant and propagating along 45° and −45° to the x axis as well, while TE 3 and TE 4 are two GMRs induced by (1, 0) and (0, 1) diffraction and propagating along the x axis and y axis, respectively. However, TM 5 and TM 6 (related to f_3) with a finite Q factor are calculated at the lattice constant of 150 μm [shown in Fig. 3(b)]. According to their electric field distributions shown in Fig. 3(c), they are GMRs induced by first-order diffraction (1, 0) and (0, 1), and propagating along the x and y directions, respectively.

Thus, quasi-BICs or GMRs with a finite Q factor can be experimentally observed when the lattice symmetry is broken [20–22,52]. However, the lattice symmetry of a 2D metasurface has more complexity and diversity than that of a 1D grating [19,20]. For example, the sizes of the air holes can be tuned (by diagonal configuration in Fig. 1, or ipsilateral configuration in Fig. 4, or only changing one air hole) to modulate the TE and/or TM BICs. In addition, the position of the air holes can be shifted either in the x axis or in the y axis to modulate the GMRs as well. But they are maintained at the oblique incidence [20].

Figure 4 shows the GMRs modulated by changing the radius of the air holes on the ipsilateral side. Here, resonance f_1 corresponds to a GMR, marked as TE 3 in Fig. 3, while f_2 is related to the two GMRs, TM 3 and TM 4. Likewise, as r_1 increases, both resonances f_1 and f_2 are blueshifted. When

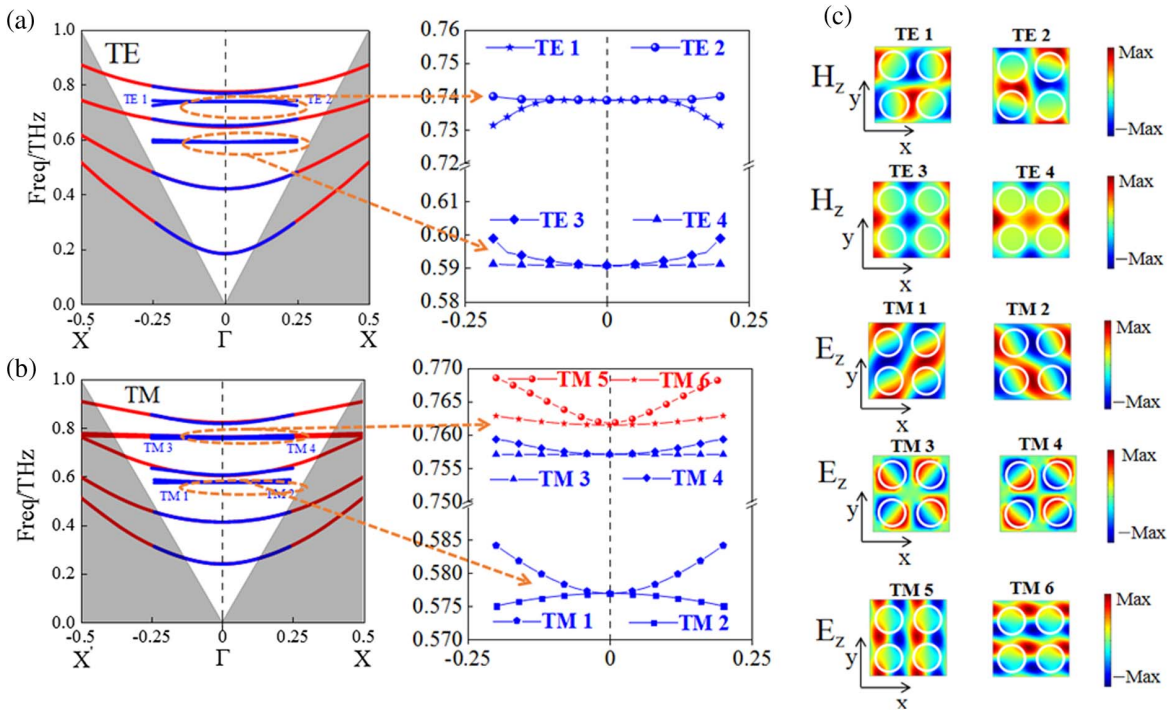

Fig. 3. Dispersion relations of (a) TE modes and (b) TM modes as a function of $k(\Lambda/\pi)$ simulated with the lattice constant of 300 μm (blue) and 150 μm (red) when $r_1 = r_2 = 55$ μm. (c) Electric fields (E_z) or magnetic fields (H_z) in the x – y plane of the 10 interested TE and TM modes at $\Gamma = 0$.

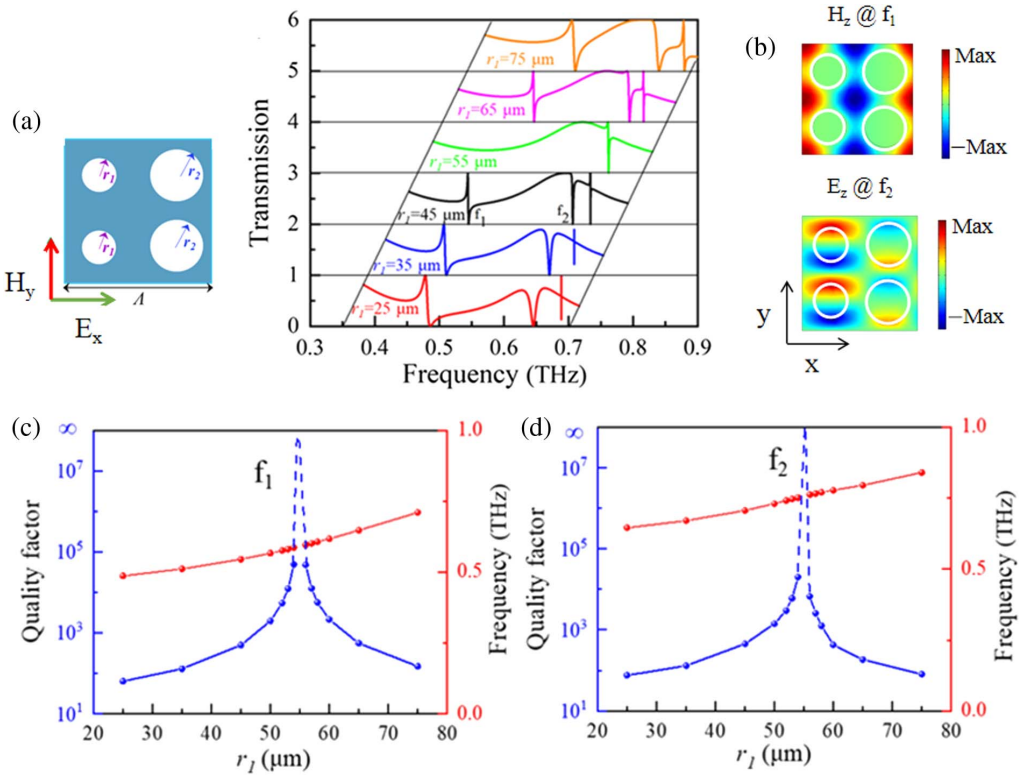

Fig. 4. (a) Calculated transmissions of the metasurface in ipsilateral configuration with different r_1 when $r_2 = 55$ μm. (b) Electric field (E_z) or magnetic field (H_z) of resonance f_1, f_2, when $r_1 = 45$ μm. (c), (d) Resonance frequencies and Q factors of f_1, f_2 with respect to r_1.

$r_1 = r_2 = 55$ μm, the two resonances disappear. Moreover, when r_1 is away from 55 μm, the Q factors of the two resonances f_1 and f_2 decrease rapidly. It can also be seen from the Q characteristics that when r_1 increases from 25 to 50 μm, the Q value of the resonance f_1 increases from 63 to 1950 and 76 to 1420 for f_2. Meanwhile, the Q value of f_1 is significantly larger than that of f_2 when r_1 is in the range of 55–75 μm. However, the Q factors of the two quasi-BICs obtained by changing the ipsilateral air holes are much smaller, as compared with the diagonal configuration; this means that the asymmetry degree of a metasurface in the ipsilateral air holes case is larger than that in a diagonal one.

3. EXPERIMENTAL RESULTS

We fabricated high-Q metasurfaces in a 2 in. high-resistivity silicon wafer (>5000 Ω cm) with a thickness of 200 μm. We chose high-resistance silicon as the building material of the metasurface because of its relatively low loss and low dispersion in the terahertz band. Here, we followed a three-step fabrication procedure. First, the silicon wafer was thinned to 150 μm, then patterned by conventional UV photolithography, and finally, etched using a deep reactive ion etching process. Since quasi-BIC resonance with higher Q factor can be calculated from the diagonal configuration, three polarization-insensitive metasurfaces with a size of 15 mm × 15 mm were prepared according to the structure shown in Fig. 1, where $r_2 = 55$ μm, and r_1 is chosen as 25, 30, and 35 μm, respectively. It should be noted here that the results in Fig. 2 are calculated by assumption of the cylindrical air holes in the structure; the real sample fabricated by deep etching is of circular truncated cone with an inclination angle about 2°, which can be seen from the sample's SEM picture in Fig. 1(b). Hence the volume of the air holes is larger than that of the cylindrical air holes, which will influence the quasi-BIC characteristics. Therefore, we recalculated the transmission spectra of the metasurface with circular truncated cone air holes, as shown in Fig. 5(a), and material loss of the high-resistance silicon (loss tangent of 0.0001) is also considered in the calculation.

Compared with the calculations of the cylindrical air hole metasurface in Fig. 2(a), when r_1 increases from 25 to 35 μm, the frequency of resonance f_1 changes little, while greatly for f_2. In addition, it is interestingly found that the Q factor of the resonance f_2 of the real metasurfaces is greatly increased compared with that of the corresponding cylindrical air hole metasurfaces. This also shows that the coupling of the unit cells in the real metasurface is greatly enhanced, which is quite beneficial for the realization of high-Q resonance. For example, when $r_1 = 25$ μm, the Q value of f_2 increases from 328 to 845, and when $r_1 = 30$ μm, the Q value of f_2 increases from 652 to 2088.

We used a high-resolution terahertz frequency-domain spectroscopy system (TeraScan 1550 from Toptica) with a focused beam incidence on the sample to measure the transmissions of three samples, and the diameter of the spot illuminating on the sample is about 6–8 mm. The measurements were done at room temperature and in the dry air condition (humidity ≤1%) to nullify the effect due to water vapor absorption, and the integration constant was set to be 300 ms. The measured transmission spectra are shown in Fig. 5(b), and enlarged views of the resonance f_2 and Fano fitting are shown in Fig. 5(c).

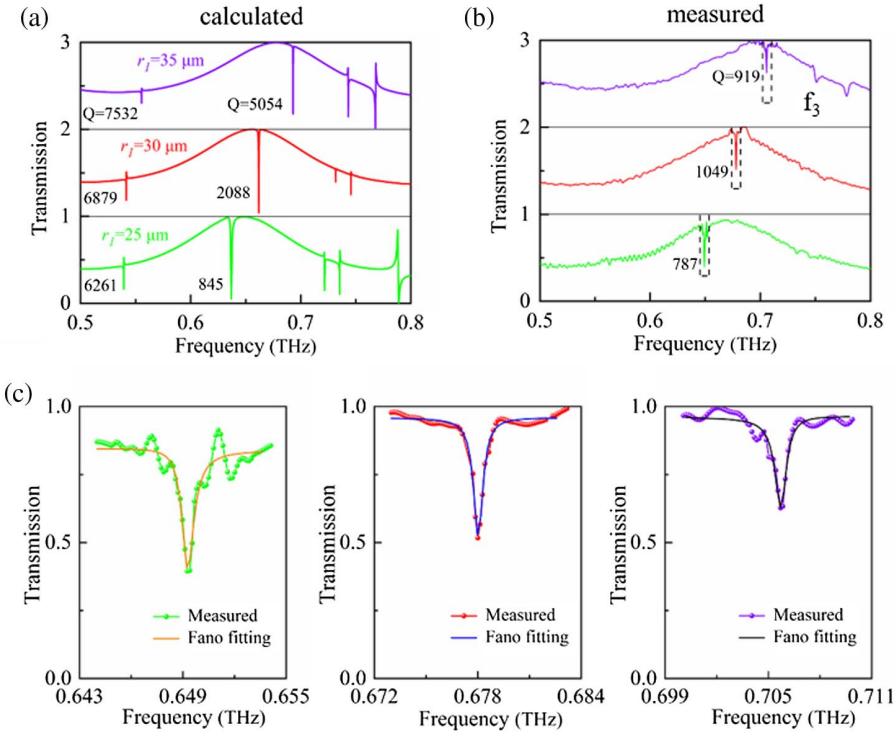

Fig. 5. (a), (b) Calculated and measured transmissions of three diagonal configuration metasurfaces with circular truncated cone air holes, loss tangent of 0.0001 is considered in calculations. (c) Three enlarged views of measured and Fano fitted resonance f_2.

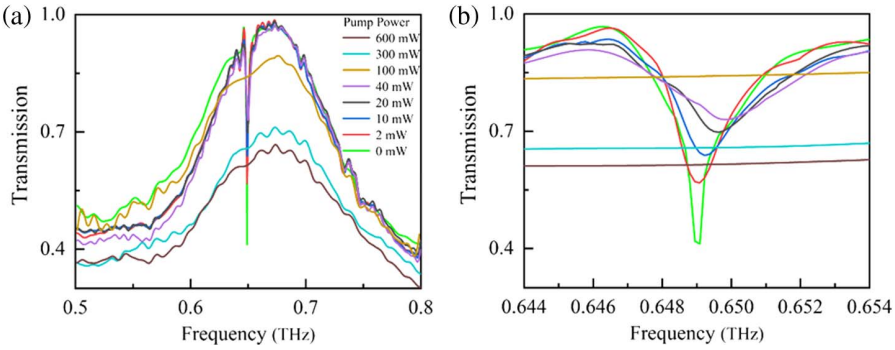

Fig. 6. (a) Transmissions of a high-Q metasurface ($r_1 = 25$ μm) irradiated at different pump powers. (b) Enlarged view of the resonance f_2.

The results show that a very weak quasi-BIC resonance f_1 at 0.565 THz was observed for the sample of $r_1 = 25$ μm, but not clearly seen in the other two samples. This may be attributed to the very high Q values of f_1 (≥6000 calculated). The higher the Q factor is, the more it is affected by the material's absorption, fabrication defects, or device size. And it may also be related to the limited spectral resolution of the measurement instrument (140 MHz). On the contrary, the strong resonance f_2 in all three samples was observed. The frequency of f_2 measured is about 10 GHz larger than the calculation result, which is caused by the inconsistency of the size between the simulation and the sample. Furthermore, as r_1 increases, the intensity of resonance f_2 measured becomes weaker, which is in good agreement with the simulation result. In addition, the measured Q value of f_2 for the sample of $r_1 = 25$ μm is 787, which is very close to our numerical calculation result of 845. And for the sample of $r_1 = 30$ μm, the calculated Q value of f_2 is 2088, while the measured Q value is 1049, which is the highest reported value for THz metasurfaces. However, for the sample of $r_1 = 35$ μm, the measured Q value decreased slightly to 919. This may be related to the limited spectral resolution of the instrument and the fabrication imperfections. Moreover, for the third resonance f_3, it is weak for the samples of $r_1 = 25$ μm and 30 μm, but strong resonance is observed when $r_1 = 35$ μm. This agrees with simulations, in which the Q factor of f_3 decreases rapidly as r_1 increases from 25 to 35 μm.

Moreover, we have also measured the samples using a backward wave oscillator THz spectrometer with spectral resolution better than 10 MHz, but all three resonances f_1, f_2, and f_3 are not observed due to low SNR of the system in the measured frequency band.

Finally, it is well known that high-Q silicon photonic crystals and metasurfaces can be used as efficient THz switches or modulators by exploring the photon-induced carrier absorption of semiconductors [14,53,54]. Here, we demonstrate an optically controllable THz modulation with remarkably reduced optical pump power by using our high-Q metasurface. In the experiment, a continuous-wave laser diode with a wavelength of 808 nm (photo energy 1.53 eV, above the bandgap of silicon 1.1 eV) was used to photoexcite the all-silicon metasurface, and the spot size on the metasurface is about 1 mm × 2 mm. Figure 6 shows transmissions of the metasurface ($r_1 = 25$ μm) when irradiated obliquely by a laser beam with different power. It is clear to see that the high-Q resonance f_2 is much more sensitive to the photoexcitation than other frequencies; hence we focus on the resonance f_2 shown in Fig. 6(b). The quasi-BIC mode is continuously modulated in terms of resonance intensity as well as Q factor by gradually tuning the photoexcitation pump power. As the pump power increases from 0 to 40 mW, the high-Q resonance of f_2 at 0.65 THz gradually becomes weak and has a slight blueshift of 1 GHz as well. And it eventually quenches at a very low pump power of 100 mW. However, a pump power of 600 mW is far from quenching a low-Q-factor mode (0.55–0.8 THz) [see Fig. 6(a)].

4. CONCLUSION

To summarize, we have proposed and experimentally demonstrated an ultra-high-Q all-silicon BIC metasurface composed of air-hole tetramer arrays. In the range of 0.4–0.9 THz, the metasurface supports two BICs originated from the GMRs, which collapse into two quasi-BIC resonances with a finite Q factor by breaking the lattice symmetry. The TE and/or TM GMRs can be flexibly modulated by changing the sizes of the air holes in both diagonal configuration and ipsilateral configuration, or by shifting the position of the air holes either in the x-axis or in the y-axis. Furthermore, we demonstrate experimentally a polarization-insensitive GMR with a record Q factor of 1049, which is 3 times higher than the highest reported in terahertz metasurfaces. Furthermore, we demonstrate a terahertz intensity modulation with very low optical pump power by exploring photon-induced carrier absorption of semiconductors. The work in this paper could pave the way not only for the research and application of high-Q terahertz metasurfaces, but also for other functional devices.

Funding. National Natural Science Foundation of China (61875179, 61875251, 12004362, 62175224).

Disclosures. The authors declare no conflicts of interest.

Data Availability. Data underlying the results presented in this paper are not publicly available at this time but may be obtained from the authors upon reasonable request.

REFERENCES

1. C. W. Hsu, B. Zhen, A. D. Stone, J. D. Joannopoulos, and M. Soljačić, "Bound states in the continuum," Nat. Rev. Mater. **1**, 16048 (2016).
2. S. I. Azzam and A. V. Kildishev, "Photonic bound states in the continuum: from basics to applications," Adv. Opt. Mater. **9**, 2001469 (2020).
3. N. J. J. van Hoof, D. R. Abujetas, S. E. T. Huurne, F. Verdelli, G. C. A. Timmermans, J. A. Sánchez-Gil, and J. G. Rivas, "Unveiling the symmetry protection of bound states in the continuum with terahertz near-field imaging," ACS Photonics **8**, 3010–3016 (2021).
4. Z. F. Sadrieva, I. S. Sinev, K. L. Koshelev, A. Samusev, I. V. Iorsh, O. Takayama, R. Malureanu, A. A. Bogdanov, and A. V. Lavrinenko, "Transition from optical bound states in the continuum to leaky resonances: role of substrate and roughness," ACS Photonics **4**, 723–727 (2017).
5. H. M. Doeleman, F. Monticone, W. den Hollander, A. Alù, and A. F. Koenderink, "Experimental observation of a polarization vortex at an optical bound state in the continuum," Nat. Photonics **12**, 397–401 (2018).
6. Y. Plotnik, O. Peleg, F. Dreisow, M. Heinrich, S. Nolte, A. Szameit, and M. Segev, "Experimental observation of optical bound states in the continuum," Phys. Rev. Lett. **107**, 183901 (2011).
7. H. Friedrich and D. Wintgen, "Interfering resonances and bound states in the continuum," Phys. Rev. A **32**, 3231–3242 (1985).
8. L. Q. Cong and R. J. Singh, "Symmetry-protected dual bound states in the continuum in metamaterials," Adv. Opt. Mater. **7**, 1900383 (2019).
9. Y. He, G. T. Guo, T. H. Feng, Y. Xu, and A. E. Miroshnichenko, "Toroidal dipole bound states in the continuum," Phys. Rev. B **98**, 161112 (2018).
10. D. R. Abujetas, N. V. Hoof, S. T. Huurne, J. G. Rivas, and J. A. Sánchez-Gil, "Spectral and temporal evidence of robust photonic bound states in the continuum on terahertz metasurfaces," Optica **6**, 996–1001 (2019).
11. K. Fan, I. V. Shadrivov, and W. J. Padilla, "Dynamic bound states in the continuum," Optica **6**, 169–173 (2019).
12. A. Kodigala, T. Lepetit, Q. Gu, B. Bahari, Y. Fainman, and B. Kanté, "Lasing action from photonic bound states in continuum," Nature **541**, 196–199 (2017).
13. M. V. Rybin, K. L. Koshelev, Z. F. Sadrieva, K. B. Samusev, A. A. Bogdanov, M. F. Limonov, and Y. S. Kivshar, "High-*Q* supercavity modes in subwavelength dielectric resonators," Phys. Rev. Lett. **119**, 243901 (2017).
14. S. Han, L. Cong, Y. K. Srivastava, B. Qiang, M. V. Rybin, A. Kumar, R. Jain, W. X. Lim, V. G. Achanta, S. S. Prabhu, Q. J. Wang, Y. S. Kivshar, and R. Singh, "All-dielectric active terahertz photonics driven by bound states in the continuum," Adv. Mater. **31**, 1901921 (2019).
15. K. Koshelev, A. Bogdanov, and Y. Kivshar, "Meta-optics and bound states in the continuum," Sci. Bull. **64**, 836–842 (2019).
16. X. Zhao, C. Chen, K. Kaj, I. Hammock, Y. Huang, R. D. Averitt, and X. Zhang, "Terahertz investigation of bound states in the continuum of metallic metasurfaces," Optica **7**, 1548–1554 (2020).
17. C. W. Hsu, B. Zhen, J. Lee, S. L. Chua, S. G. Johnson, J. D. Joannopoulos, and M. Soljačić, "Observation of trapped light within the radiation continuum," Nature **499**, 188–191 (2013).
18. D. R. Abujetas, J. Olmos-Trigo, and J. A. Sanchez-Gil, "Tailoring accidental double bound states in the continuum in all-dielectric metasurfaces," Adv. Opt. Mater. **10**, 2200301 (2022).
19. A. C. Overvig, S. Shrestha, and N. F. Yu, "Dimerized high contrast gratings," Nanophotonics **7**, 1157–1168 (2018).
20. W. Q. Shi, J. Q. Gu, X. Y. Zhang, Q. Xu, J. G. Han, Q. L. Yang, L. Q. Cong, and W. L. Zhang, "Terahertz bound states in the continuum with incident angle robustness induced by a dual period metagrating," Photonics Res. **10**, 810–819 (2022).
21. F. Wu, J. J. Wu, Z. W. Guo, H. T. Jiang, Y. Sun, Y. H. Li, J. Ren, and H. Chen, "Giant enhancement of the Goos-Hanchen shift assisted by quasibound states in the continuum," Phys. Rev. Appl. **12**, 014028 (2019).
22. S. Murai, D. R. Abujetas, L. B. Liu, G. W. Castellanos, V. Giannini, J. A. Sanchez-Gil, K. Tanaka, and J. G. Rivas, "Engineering bound states in the continuum at telecom wavelengths with non-Bravais lattices," Laser Photonics Rev., 2100661 (2022).
23. Y. K. Srivastava, M. Gupta, and R. Singh, "Terahertz sensing of 7 nm dielectric film with bound states in the continuum metasurfaces," Appl. Phys. Lett. **115**, 151105 (2019).
24. A. Tittl, A. Leitis, M. Liu, F. Yesilkoy, D. Y. Choi, D. N. Neshev, Y. S. Kivshar, and H. Altug, "Imaging-based molecular barcoding with pixelated dielectric metasurfaces," Science **360**, 1105–1109 (2018).
25. F. Yesilkoy, E. R. Arvelo, Y. Jahani, M. Liu, A. Tittl, V. Cevher, Y. Kivshar, and H. Altug, "Ultrasensitive hyperspectral imaging and biodetection enabled by dielectric metasurfaces," Nat. Photonics **13**, 390–396 (2019).
26. X. Chen and W. Fan, "Ultrahigh-*Q* toroidal dipole resonance in all-dielectric metamaterials for terahertz sensing," Opt. Lett. **44**, 5876–5879 (2019).
27. C. Huang, C. Zhang, S. Xiao, L. Ge, Y. Kivshar, and Q. Song, "Ultrafast control of vortex microlasers," Science **367**, 1018–1021 (2020).
28. M. S. Hwang, H. C. Lee, K. H. Kim, K. Y. Jeong, S. H. Kwon, K. Koshelev, Y. Kivshar, and H. G. Park, "Ultralow-threshold laser using super-bound states in the continuum," Nat. Commun. **12**, 4135 (2021).
29. L. Carletti, K. Koshelev, C. D. Costntino, D. Angelis, and Y. Kivshar, "Giant nonlinear response at the nanoscale driven by bound states in the continuum," Phys. Rev. Lett. **121**, 033903 (2018).
30. K. Koshelev, Y. Tang, K. Li, D. Y. Choi, G. Li, and Y. Kivshar, "Nonlinear metasurfaces governed by bound states in the continuum," ACS Photonics **6**, 1639–1644 (2019).
31. V. A. Fedotov, M. Rose, S. L. Prosvirnin, N. Papasimakis, and N. I. Zheludev, "Sharp trapped-mode resonances in planar metamaterials with a broken structural symmetry," Phys. Rev. Lett. **99**, 147401 (2007).
32. W. Cao, R. Singh, A. Al-Naib, M. He, J. Taylor, and W. Zhang, "Low-loss ultra-high-*Q* dark mode plasmonic Fano metamaterials," Opt. Lett. **37**, 3366–3368 (2012).
33. B. X. Han, X. J. Li, C. S. Sui, J. Y. Diao, X. F. Jing, and Z. Hong, "Analog of electromagnetically induced transparency in an E-shaped all-dielectric metasurface based on toroidal dipolar response," Opt. Mater. Express **8**, 2197–2207 (2018).
34. Z. H. Wang, L. L. Chen, X. J. Li, T. T. Lang, X. F. Jing, and Z. Hong, "Analogue of electromagnetically induced transparency with ultra-narrow bandwidth in a silicon terahertz metasurface," Opt. Mater. Express **11**, 1943–1952 (2021).
35. Y. Yang, I. I. Kravchenko, D. P. Briggs, and J. Valentine, "All-dielectric metasurface analogue of electromagnetically induced transparency," Nat. Commun. **5**, 5753 (2014).
36. S. Campione, S. Liu, L. I. Basilio, L. K. Warne, W. L. Langston, T. S. Luk, J. R. Wendt, J. L. Reno, G. A. Keeler, I. Brener, and M. B. Sinclair, "Broken symmetry dielectric resonators for high quality factor Fano metasurfaces," ACS Photonics **3**, 2362–2367 (2016).
37. S. Yuan, X. Qiu, C. Cui, L. Zhu, Y. Wang, Y. Li, J. Song, Q. Huang, and J. Xia, "Strong photoluminescence enhancement in all-dielectric Fano metasurface with high quality factor," ACS Nano **11**, 10704–10711 (2017).
38. B. Auguié and W. L. Barnes, "Collective resonances in gold nanoparticle arrays," Phys. Rev. Lett. **101**, 143902 (2008).
39. V. G. Kravets, F. Schedin, and A. N. Grigorenko, "Extremely narrow plasmon resonances based on diffraction coupling of localized plasmons in arrays of metallic nanoparticles," Phys. Rev. Lett. **101**, 087403 (2008).
40. M. S. Bin-Alam, O. Reshef, Y. Mamchur, M. Z. Alam, G. Carlow, J. Upham, B. T. Sullivan, J. M. Ménard, M. J. Huttunen, R. W. Boyd, and K. Dolgaleva, "Ultra-high-*Q* resonances in plasmonic metasurfaces," Nat. Commun. **12**, 974 (2021).
41. K. Koshele, S. Lepeshov, M. Liu, A. Bogdanov, and Y. Kivshar, "Asymmetric metasurfaces with high-Q resonances governed by bound states in the continuum," Phys. Rev. Lett. **121**, 193903 (2018).

42. S. T. Ha, Y. H. Fu, N. K. Emani, Z. Y. Pan, R. M. Bakker, R. Paniagua-Dominguez, and A. I. Kuznetsov, "Directional lasing in resonant semiconductor nanoantenna arrays," Nat. Nanotechnol. **13**, 1042–1047 (2018).
43. Z. J. Liu, Y. Xu, Y. Lin, J. Xiang, T. H. Feng, Q. T. Cao, J. T. Li, S. Lan, and J. Liu, "High-*Q* quasibound states in the continuum for nonlinear metasurfaces," Phys. Rev. Lett. **123**, 253901 (2019).
44. C. C. Cui, C. B. Zhou, S. Yuan, X. Z. Qiu, L. Q. Zhu, Y. X. Wang, Y. Li, J. W. Song, Z. Huang, Y. Wang, C. Zeng, and J. S. Xia, "Multiple Fano resonances in symmetry breaking silicon metasurface for manipulating light emission," ACS Photonics **5**, 4074–4080 (2018).
45. Q. Yang, D. Wang, S. Kruk, M. Liu, I. Kravchenko, J. Han, Y. Kivshar, and I. Shadrivova, "Topology-empowered membrane devices for terahertz photonics," Adv. Photonics **4**, 046002 (2022).
46. Q. Yang, S. Kruk, Y. Xu, Q. Wang, Y. K. Srivastava, K. Koshelev, I. Kravchenko, R. Singh, J. Han, Y. Kivshar, and I. Shadrivov, "Mie-resonant membrane Huygens' metasurfaces," Adv. Funct. Mater. **30**, 1906851 (2020).
47. L. Li, H. Zhao, C. Liu, L. Li, and T. J. Cui, "Intelligent metasurfaces: control, communication and computing," eLight **2**, 7 (2022).
48. D. Lee, S. So, G. Hu, M. Kim, T. Badloe, H. Cho, J. Kim, H. Kim, C. W. Qiu, and J. Rho, "Hyperbolic metamaterials: fusing artificial structures to natural 2D materials," eLight **2**, 1 (2022).
49. M. Galli, S. L. Portalupi, M. Belotti, L. C. Andrean, and T. F. Lrauss, "Light scattering and Fano resonances in high-*Q* photonic crystal nanocavities," Appl. Phys. Lett. **94**, 071101 (2009).
50. I. S. Maksymov and A. E. Miroshnichenko, "Active control over nanofocusing with nanorod plasmonic antennas," Opt. Express **19**, 5888–5894 (2011).
51. S. S. Wang and R. Magnusson, "Theory and applications of guided-mode resonance filters," Appl. Opt. **32**, 2606–2613 (1993).
52. Z. Yu, H. Chen, J. Liu, X. Jing, X. Li, and Z. Hong, "Guided mode resonance in planar metamaterials consisting of two ring resonators with different size," Chin. Phys. B **26**, 077804 (2017).
53. T. Chen, P. Liu, J. Liu, and Z. Hong, "A terahertz photonic crystal cavity with high *Q*-factors," Appl. Phys. B **115**, 105–109 (2014).
54. A. Kumar, M. Gupta, P. Pitchappa, T. C. Tan, U. Chattopadhyay, G. Ducournau, N. Wang, Y. Chong, and R. Singh, "On-chip active control of ultra-high-*Q* terahertz photonic topological cavities," Adv. Mater. **34**, 2202370 (2022).